CrossMark

ORIGINAL PAPER

Biobased aerogels with different surface charge as electrolyte carrier membranes in quantum dot-sensitized solar cell

Maryam Borghei [ORCID] · **Kati Miettunen** · **Luiz G. Greca** · **Aapo Poskela** ·
Janika Lehtonen · **Sakari Lepikko** · **Blaise L. Tardy** · **Peter Lund** ·
Vaidyanathan (Ravi) Subramanian · **Orlando J. Rojas**

Abstract Biobased aerogels were used as environmentally friendly replacement for synthetic polymers as electrolyte carrier membranes in quantum dot-sensitized solar cell (QDSC). Integration of polymeric components in solar cells has received increased attention for sustainable energy generation. In this context, biobased aerogels were fabricated to apply as freestanding, porous and eco-friendly electrolyte holding membranes in QDSC. Bacterial cellulose (BC), cellulose nanofibers (CNF), chitin nanofibers (ChNF) and TEMPO-oxidized CNF (TOCNF) were selected because of their fibrilar structures and water-holding capability to investigate their inherent differences in terms of surface groups and electrostatic charge on the electrolyte redox reaction and the photocell function. BC, CNF, ChNF and TOCNF were selected due to different surface functional groups (hydroxyl, *N*-acetylglucosamine and carboxyl units) and fibrilar structures that can form highly interconnected and robust network. These aerogels enabled easy handling, effective electrolyte filling and efficient redox reactions, while keeping the solar cell performance *on par* to that of traditional reference cells without membranes. The aerogel membranes maintained the photocell performance since they took only a very small space of the electrolyte volume, which allowed efficient charge transfer. The results indicated that aerogels did not interfere with the cell operation, as confirmed by quartz crystal microgravimetry with bio-interphases in contact with the polysulfide-based electrolyte. The electrochemical measurements also suggested that the respective functional groups (hydroxyl, *N*-acetylglucosamine and carboxyl units) did not interfere with the redox reaction of the polysulfide electrolyte.

Keywords Cellulose nanofibers · TEMPO-oxidized cellulose · Bacterial cellulose · Chitin nanofiber · Solar cells · Electrolyte membrane

M. Borghei (✉) · K. Miettunen · L. G. Greca ·
J. Lehtonen · B. L. Tardy · V. (Ravi)Subramanian ·
O. J. Rojas
Department of Bioproducts and Biosystems, School of
Chemical Engineering, Aalto University, 00076 Espoo,
Finland
e-mail: maryam.borghei@aalto.fi

K. Miettunen · A. Poskela · S. Lepikko ·
P. Lund · O. J. Rojas
Department of Applied Physics, School of Science, Aalto
University, 00076 Espoo, Finland

V. (Ravi)Subramanian
Chemical and Materials Engineering, University of
Nevada, Reno, NV 89557, USA

Introduction

Recently, nanocellulose has become an attractive component for electronic and photovoltaic devices from ink and electrolyte formulation to self-standing and transparent substrates (Zhu et al. 2014; Hoeng et al. 2016). Their integration in solar cell technologies stems from benefits related to the fact that they are fully recyclable, scalable, and environmentally-friendly (Zhou et al. 2013; Zhu et al. 2016). Quantum dot-sensitized solar cells (QDSC), are third generation photocell technology utilizing quantum dot semiconductors as sensitizers because of their quantum confinement effect and multiple exciton generation (Jiang et al. 2016; Shen et al. 2016). Despite high theoretical conversion efficiency of QDSC, one of the major problems is the limited conversion efficiency due to the insufficient light absorption of QDs and recombination of electrons and holes at the QD-electrolyte interface. In recent years, a lot of efforts have been conducted to expand the light absorption range within the solar spectrum by tuning the photo-electrode via selection of various QDs with different bandgaps. As presented in Table 1, conversion efficiencies were improved significantly using integrated QD systems from almost 0.5% in conventional CdS-based photocells (Duan et al. 2014, 2015a), to 2–6% in CdS/CdSe systems (Chen et al. 2013; Kim et al. 2014; Huo et al. 2015), and finally reaching to 9–11% using CdSeTe (Feng et al. 2016a, b; Jiang et al. 2016; Wei et al. 2016). In spite of the progress in the photoelectrode, another prevalent challenges is the evaporation of electrolyte solvent and the loss of electrolyte and performance (Duan et al. 2015b; Sharma et al. 2016). Therefore, replacement of common liquid electrolytes with solid-based or quasi-solid hole-transport material is a feasible option. As presented in Table 1, polymer-based PEO-PVDF (Yang and Wang 2015), plastic crystal succinonitrile (Duan et al. 2015a), PEDOT (Xia et al. 2008), inorganic/organic hole-transport materials (Chang et al. 2010), as well as inorganic p-type CuSCN (Larramona et al. 2006) have been applied as solid-state alternatives. However, there are challenges to overcome the low ion mobility and difficulties in electrolyte filling of the mesoporous oxides. On the other hand, quasi-solid state electrolytes have been reported by introducing gelling agents to common polysulfide electrolytes such as fumed silica nanoparticles (Kumar et al. 2015; Wei

et al. 2016), dextran (Chen et al. 2013), hydroxystearic acid (Huo et al. 2015), polyacrylamides (PAAM) (Yu et al. 2010; Narayanan et al. 2013), sodium polyacrylate (PAAS) (Feng et al. 2016a) or polyethylene glycol (PEG) (Du et al. 2015). More recently, bio-organic components such as agar (Raphael et al. 2017), carboxymethyl cellulose (CMC) (Feng et al. 2016b), methylcellulose (Mingsukang et al. 2017) and Konjac glucomannan (Wang et al. 2013) have been considered.

Considering the importance of developing natural-based components in QDSC, we applied different polysaccharide materials, namely, bacterial cellulose (BC), cellulose nanofibers (CNF), TEMPO-oxidized cellulose nanofibers (TOCNF) and chitin nanofibers (ChNF), as carriers for the polysulfide electrolyte (Fig. 1). Specially, the respective nanofibers form three-dimensional, highly interconnected networks upon controlled drying. This enables efficient trapping of the liquid electrolyte in the soft cages of the fibrilar network, which is expected to provide electrolyte accessibility and ionic conductivity. In addition, their abundant surface hydroxyl groups endow hygroscopic and water-holding properties, as well as metal-ion coordination capabilities, rendering better attachment with porous TiO_2 films (Feng et al. 2016b). In this work, the classical architecture of a QDSC consists of CdS-sensitized photoanode, Pt counter electrode and, polysulfide redox electrolyte containing S^{-2}/S_n^2 redox couples was used as shown in Fig. 1. Here, we would like to specifically investigate the influence of the different surface functional groups (hydroxyl, N-acetylglucosamine and carboxyl units) on polysulfide redox reaction via quartz crystal microgravimetry and electrochemical measurements. The fiber network obtained were comparable for all fiber sources while the surface charges were significantly different: bacterial cellulose having the least charged groups, TOCNF with strongly negative surface charge and ChNF containing high positive charges. Thus, we not only evaluate nanofiber materials as high water holding aerogels but also benchmark the effects of surface charges on electrolyte transport and electrochemical polysulfide redox reaction.

Table 1 Summary of QDSC performance parameters using different photoelectrode, counter electrode and electrolyte components. The QDSC performance parameters for the traditional reference cells (liquid-electrolyte) are presented in parentheses

Polymer used in electrolyte	Photoelectrode	Counter electrode	Electrolyte	J_{sc} (mA/ cm^2)	V_{oc} (V)	η (%)	FF (%)	References
PEO-PVDF	FTO/TiO$_2$/CdSe/ZnS	FTO/Pt	TMAS[*]/S	–	–	–	–	Yang and Wang (2015)
3% Fumed silica	FTO/TiO$_2$/CdSeTe/TiCl$_4$/ZnS	Brass/Cu$_2$S	–	22.21 (21.18)	0.710 (0.643)	11.23 (8.73)	71.2 (64.1)	Wei et al. (2016)
20%PVP	FTO/TiO$_2$/CdSeTe/TiCl$_4$/ZnS/SiO2	FTO/Cu$_2$S	2 M Na$_2$S/S 2 M KCl	20.49 (20.58)	0.723 (0.694)	9.77 (9.06)	66.0 (63.4)	Jiang et al. (2016)
CMC-Na	FTO/TiO$_2$/CdSeTe	FTO/Cu$_2$S	2 M Na$_2$S/S	21.89 (22.32)	0.667 (0.655)	9.21 (9.18)	63.0 (62.8)	Feng et al. (2016b)
15% PAAS	FTO/TiO$_2$/CdSeTe/ZnS	FTO/Cu$_2$S	2 M Na$_2$S/S	20.49 (20.98)	0.662 (0.655)	8.46 (8.44)	62.4 (61.4)	Feng et al. (2016a)
15% PEG	FTO/TiO$_2$/TiCl$_4$/CdSe/ZnS/SiO$_2$	FTO/Cu$_2$S	1 M Na$_2$S/S	15.81 (15.39)	0.643 (0.604)	6.81 (5.87)	66.9 (63.1)	Du et al. (2015)
20%PEGDME-fumed silica NP	FTO/ZnO/CdS/CdSe	FTO/Pt/CNT-RGO	2 M S/0.5 M Na$_2$S/0.2 M KCl in MeOH:W	17.84 (17.32)	0.719 (0.732)	5.45 (5.69)	42 (45)	Kim et al. (2014)
Konjac glucomannan	FTO/TiO$_2$/CdS/CdSe/ZnS	Brass/Cu$_2$S	1 M Na$_2$S/S	12.76 (13.05)	0.503 (0.512)	4.06 (4.22)	63 (63)	Wang et al. (2013)
PAM	FTO/TiO$_2$/CdS/CdSe/ZnS	Brass/Cu$_2$S	1 M Na$_2$S/S	12.4 (12.8)	0.534 (0.548)	4.0 (4.3)	60.1 (61)	Yu et al. (2010)
4.1% Fumed silica	FTO/TiO$_2$/TiCl$_4$/CdS/Ag nanorod	FTO/MWCNT	0.1 M Na$_2$S (Me/W)	10.43 (11.67)	0.920 (1.021)	3.65 (4.27)	38 (35.8)	Kumar et al. (2015)
15% Dextran	FTO/TiO$_2$/TiCl$_4$/CdS/CdSe	FTO/Pt	1 M Na$_2$S/S KCl	15.86 (16.72)	0.466 (0.482)	3.23 (3.69)	44 (46)	Chen et al. (2013)
Agar/glycerol	FTO/TiO$_2$/CdS/ZnS and CuInS$_2$/ZnS	FTO/Cu$_2$S/RGO	2M Na$_2$S/S	13.51 (10.95)	0.575 (0.587)	2.98 (2.80)	38 (43)	Raphael et al. (2017)
3% 12-hydroxystearic acid	FTO/TiO$_2$/CdS/CdSe	FTO/Pt	1 M Na$_2$S/S 0.1 M NaOH	12.18 (14.42)	0.49 (0.47)	2.40 (2.88)	42 (41)	Huo et al. (2015)
methylcellulose	FTO/TiO$_2$/CdS/ZnS/SiO$_2$	1 M S/Na$_2$S	Na$_2$S/S	7.30 (4.66)	0.56 (0.51)	1.42 (0.78)	34 (33)	Mingsukang et al. (2017)
Plastic crystal succinonitrile	FTO/TiO$_2$/CdS	FTO/CoSe	Na$_2$S	3.65	0.670	1.29	52.7	Duan et al. (2015a)
PVP	FTO/TiO$_2$/CdS	FTO/CoSe	Na$_2$S/S (1:10)	2.84	0.67	0.55	28.9	Duan et al. (2014)
Polyacrylamide and CuPc	FTO/ZnS/CdS/ZnS/C-dot	FTO/MWCNT	–	–	–	0.34 (0.35)	–	Narayanan et al. (2013)
BC, CNF, ChNF, TOCNF	FTO/TiO$_2$/CdS	FTO/Pt	0.5 M Na$_2$S/S 0.1 M KCl in MeOH:W	5.1 (4.8)	0.604 (0.590)	0.52 (0.58)	17.1 (20.3)	This work

[*]Tetramethylammonium sulfate
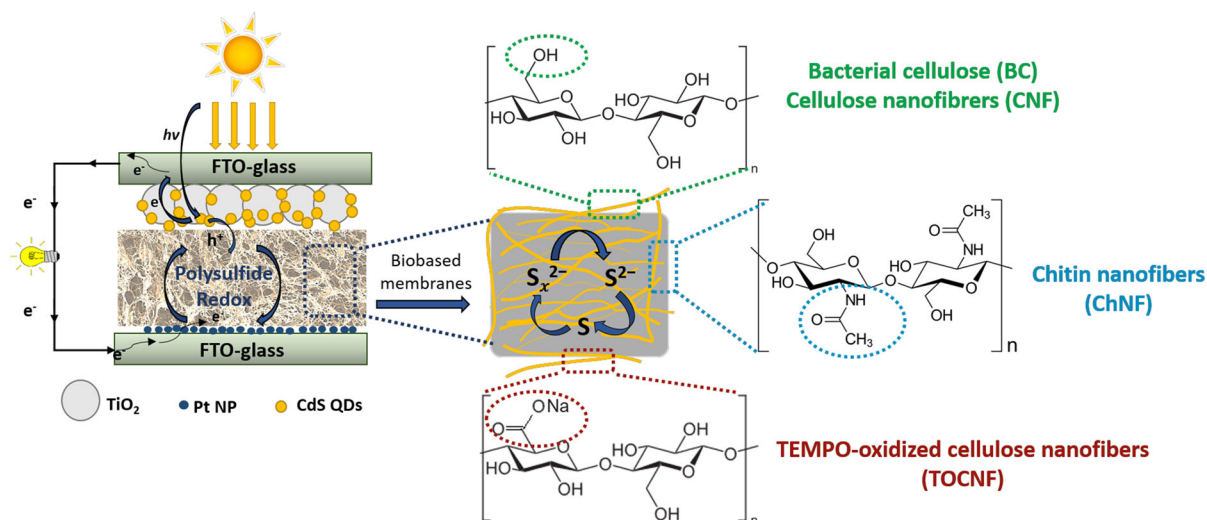
Fig. 1 Schematic illustration of biobased aerogels as electrolyte-retaining membranes in a QDSC containing CdS-sensitized photoelectrode and Pt counter electrode on fluorine-doped tin oxide (FTO)-glass substrates. The magnified aerogel illustrates the electrolyte redox ions at the interface of nanofibers with different surface charges and groups (hydroxyl groups in BC and CNF, amide groups in ChNF and carboxyl groups in TOCNF)

Experimental

Biobased aerogels

Bacterial cellulose (BC) was harvested as pellicles that were grown at the air–liquid interface of culture media contained in Erlenmeyer flasks that were seeded with a BC-producing bacterium, *Komagataeibacter medellinensis*. The flasks were incubated for 2 days at 28 °C. The BC pellicles were removed and purified by treatment with 0.1 M NaOH (60 °C, 2 h) followed by washing with water.

CNF was prepared from never dried bleached wood (birch) fibers by fibrillation from an aqueous dispersion (2% solid content) after six passes through a high-pressure M-110 P fluidizer (Microfluidics corp. Newton, MA, USA). TEMPO-oxidized cellulose nanofibrils (TOCNF) were prepared according to our previous report (Orelma et al. 2016). Purified chitin flakes from shrimp shells were purchased from Sigma Aldrich, with the degree of acetylation (DA) of $\sim$ 72%. Chitin nanofibers (ChNF) were prepared by disintegration of chitin flakes dispersion (1% solids in HCl aqueous solution at pH 4) after six passes through the fluidizer. For aerogel preparation, 40 mL of 0.1% dispersion of CNF, ChNF and TOCNF were dispersed using tip sonication (Branson 450 EC sonicator) for 10 min and 10% amplitude. The respective dispersion was vacuum filtered through a hydrophilic polyvinylidene fluoride filter (0.45 μm, GVWP, Millipore) until a gel-cake was formed, and then it was transferred to a glass petri dish and the filter paper was peeled off according to a previous report (Toivonen et al. 2015). Subsequently, the free-standing gel-cake was subjected to solvent exchange with ethanol (three times) and tert-butanol (three times) followed by freezing at − 80 °C and freeze-drying using Labconco system (74200 series). BC aerogels were prepared from the as-obtained wet BC membranes after solvent exchange and freeze-drying (Fig. S1).

Electrode preparation

The photoelectrode substrates containing TiO$_2$ layer were made on fluorine-doped tin oxide (FTO) glass (TEC-15, Pilkington) according to our previous report (Miettunen et al. 2014). Three layers of TiO$_2$ were deposited using screen-printer (AT-60PD, ATMA): the first two layers of paste were small TiO$_2$ particles ($\sim$ 20 nm, Dyesol, 18NR-T) and the last layer using TiO$_2$ paste with larger light scattering particles ($\sim$ 150–250 nm, Dyesol, WER2-0). After printing, they were sintered in an oven at 450 °C for 30 min. The resulting porous TiO$_2$ layers were ca. 13–14 μm in thickness and 40 mm^2 in area. Electrodes with blocking layer (TiCl$_4$) were also prepared in order to

restrict light absorption in areas other than the printed TiO$_2$. The catalyst for the counter electrode was prepared by spreading 4 μL of 5 mM H$_2$PtCl$_6$ in 2-propanol on a clean FTO-substrate, followed by treatment at 390 °C for 20 min.

CdS sensitizing

First, FTO-glass substrates containing TiO$_2$ layers were kept in a vacuum oven at 60 °C for ∼ 30 min to remove the moisture. Then, CdS nanoparticle deposition was carried out via Successive Ionic Layer Adsorption and Reduction (SILAR) (Pathak et al. 2016) by dipping repetitively for 60 s in solution of 0.1 M Cd(NO$_3$)$_2$ in ethanol and washing in pure ethanol. Then deposition was followed by immersing in 0.1 M Na$_2$S in methanol and final rinsing in pure methanol. The SILAR process was repeated for several cycles until a stable and good coverage was reached. The deposition was evaluated using UV–Vis spectra of the sensitized substrate (absorption reach to near 0.7 at 350 nm as shown in Fig. 4a).

Photocell assembly

The given aerogels were cut using a laser cutter set to low power (Epilog 35 W Zing) to obtain a size slightly larger than the geometry of the photoactive part (15 mm × 5 mm). 8 μL of the electrolyte was pipetted on the aerogel slice and sandwiched between the photo- and counter electrodes with a 60 μm Surlyn 1702 frame foil as spacer. A mixed solution of 0.5 M Na$_2$S/S and 0.1 M KCl in water: methanol (3:7) was used as the electrolyte. This solvent mixture was chosen so that dissociation takes place in the polar component while the organic, alcohol phase reduces the surface tension to improve the penetration of the electrolyte into the mesoporous TiO$_2$ layer (Lee and Chang 2008).

Photovoltaic performance and other characterization

Scanning electron microscopy (SEM) was performed on the aerogels with a field emission Zeiss Sigma VP at 2 kV. Rigaku SmartLab X-ray diffractometer (XRD) with Cu anode was used to obtain the QD particle size. UV–Vis spectra were collected using a Shimadzu UV 2550 from 800 to 250 nm wavelength.

Fourier transform infrared (FTIR) spectroscopy was carried out with a Nicolet 380 spectrometer. Zeta potential of the nanofibers was measured from 0.1% dispersion using a Doppler Electrophoretic Light Scattering Analyzer Malvern Zeta sizer Nano ZS 90. Photovoltaic measurements were conducted with the photocells by using a Peccell PEC-01 class A with a xenon lamp. The simulator generated an output equivalent to solar output in AM1.5G (1 Sun). The electrochemical impedance spectroscopy (EIS) measurements were carried out using Zahner Zennnium potentiostat.

To understand the interactions between the electrolyte and the nanofibers used in the membranes in the photocells, quartz crystal microgravimetry (QCM-D) were carried out using Q-Sense E4 apparatus (Västra Frölunda, Sweden). Gold-coated quartz crystals were used as substrates. The quartz crystals were first cleaned with 10% NaOH for 20 s, rinsed sequentially with Milli-Q and ethanol, dried under nitrogen flow, and treated with UV/ozone for 15 min. Then, they were dip-coated with 30% polyethyleneimine (PEI) during 15 min, followed by washing thoroughly with Milli-Q and drying with N$_2$ flow. The nanofiber dispersions (0.1%) were sonicated for 10 min (10% amp, 1 s on/off cycles) using a micro-tip and an ice bath to avoid excessive heating of the sample. Prior to the spin coating, the substrates were cleaned with Milli-Q water by drop casting on the substrates and spun at 3000 rpm, 1000 rpm/s, during 30 s. Finally, the nanofiber suspensions were spin coated on the substrates at 3000 rpm, with a 1000 rpm/s ramp, during 90 s. Prior to the QCM measurement, the samples were rinsed with Milli-Q, gently dried with N$_2$ flow, and placed in the oven at 80 °C during 10 min. The coated substrates were placed in the QCM-D device and measurements started after pumping water at 0.1 mL/min for ca. 1 h until a stable signal was obtained (drift less than 0.1 Hz min^{-1}). Then, the electrolyte was pumped into the compartments at a flow rate of 0.05 mL/min. After ca. 90 min, the electrolyte was rinsed with water at 0.1 mL/min. The measurements were repeated at least two times.

The electrochemical redox reaction was carried out using an Autolab PGSTAT12 potentiostat controlled by the GPES software. The glassy carbon electrodes (GCE, 0.196 cm^2) were polished and then modified by casting 30 μL of 0.5% of nanofibril dispersion and left to dry overnight. Cyclic voltammograms (CV) were

recorded in a 3-electrode cell compartment using Ag/AgCl as a reference electrode, Pt counter electrode and modified GCE as working electrode in the polysulfide electrolyte.

Results and discussion

### Biobased aerogels and CdS-sensitized TiO$_2$ photoanode

Four types of biobased aerogels based on BC, CNF, TOCNF and ChNF were prepared via solvent-exchange and freeze-drying. As can be seen in Fig. 2, all of them contained randomly oriented, interconnected fibrils and bundles. BC aerogel (Fig. 2a) formed distinctive three-dimensional network of highly individualized fibrils. CNF (Fig. 2b) showed lower degree of fibrillation compared to TOCNF (Fig. 2c), which was the result of more extensive fibrillation and finer fibril size due to the TEMPO-oxidization treatment. Finally, ChNF (Fig. 2d), presented an intermediate fibrillation because protonation of aminoacetyl groups in acidic condition (pH 4) results in more positive surface charge and electrostatic repulsion to enhance fibrillation. The porous network of the dried aerogels

benefited from the sequential solvent exchange (water to ethanol to tert-butanol) that lowered the surface tension and significantly reduced the capillary forces prevalent during drying (Sehaqui et al. 2011). Other choices of solvent exchange (for example water to isopropanol to octane) followed by drying in room conditions (Toivonen et al. 2015) were applied but resulted in more compact structures (Fig. S2) and were not considered further.

The FTIR spectra were obtained to investigate the surface functional groups. Figure 3 shows OH stretching vibration for BC, CNF and TOCNF at 3343–3349 cm^{-1}, while in the case of ChNF it was slightly shifted to 3437 cm^{-1} (Sharma et al. 2012; Du et al. 2016). The peak in the 2878–2897 cm^{-1} region in all the samples was assigned to the C–H vibration (from CH$_2$) (Missoum et al. 2013). For TOCNF, a clear peak was noted at 1608 cm^{-1}, assigned to the C=O stretching of the sodium carboxylate groups, COONa (Fujisawa et al. 2011). The band around 1407 cm^{-1} resulted from the C–O symmetric stretching of dissociated carboxylate groups. Likewise, a small band at 1726 cm^{-1} was assigned to C=O stretching of carboxylate units forming hydrogen bonds (Du et al. 2016). For ChNF, the typical peaks of the α-chitin fingerprint were appeared
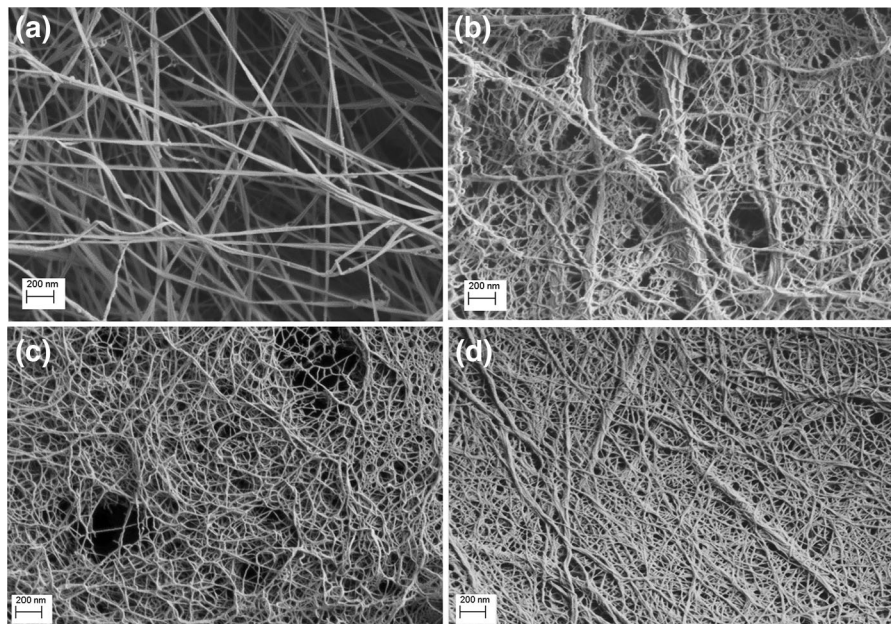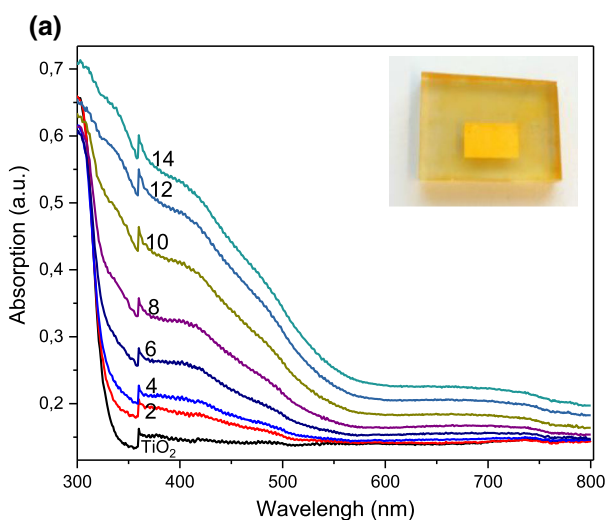

Fig. 2 SEM micrograph of biobased aerogels obtained after solvent exchange of hydrogel membranes with ethanol and tert-butanol followed by freeze draying: **a** BC), **b** CNF, **c** TOCNF and **d** ChNF
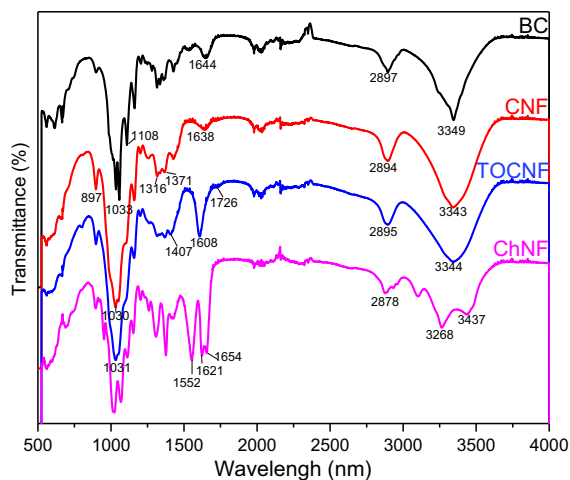
Fig. 3 FTIR spectra of the aerogel membranes prepared from BC, CNF, TOCNF, ChNF (top to bottom)

including –NH stretching vibration at 3268 cm^{-1}, the C=O region with three sharp bands from the amide I at 1654 and 1621 cm^{-1} and amide II at 1552 cm^{-1} (Liang et al. 2007; Ifuku et al. 2009).

To obtain the photoelectrodes, CdS nanoparticles were deposited on mesoporous TiO$_2$ layer via SILAR process. The respective UV–Vis absorption spectra (Fig. 4a), indicted that the peak wavenumber red shifted and the corresponding absorption intensity was enhanced with the number of SILAR cycles. The photo ima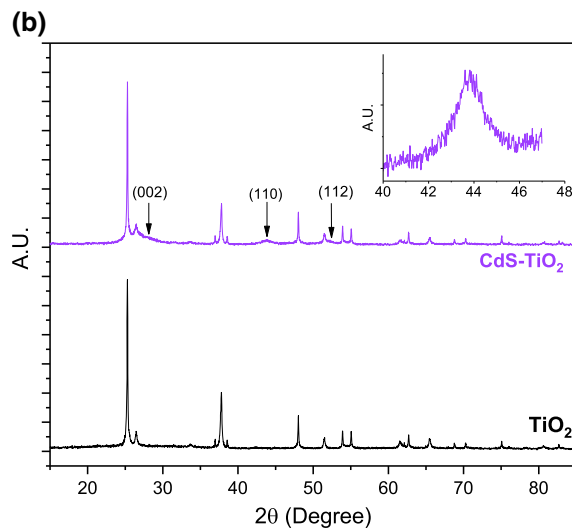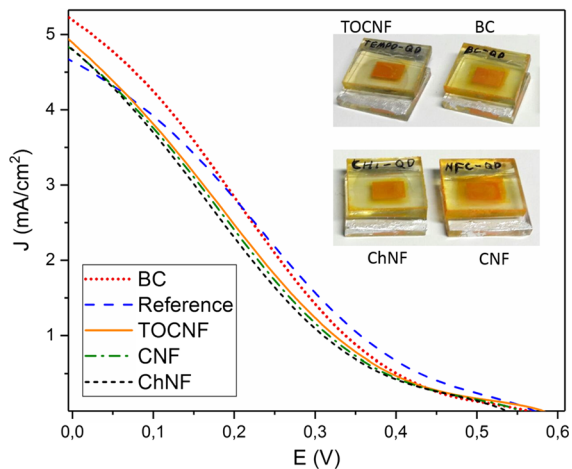ge of the QD-sensitized electrode is demonstrated in the inset of Fig. 4a. A clear difference in the surface features was observed in SEM micrographs (Fig. S3) showing that CdS QDs covered and filled the pores of the TiO$_2$ layer compared to the bare TiO$_2$. The XRD pattern of CdS-sensitized TiO$_2$ electrodes (Fig. 4b) showed peaks at 2θ values of 26.5°, 43.7°, 52.9°, assigned to (002), (110), (112) planes of hexagonal CdS (JCPDS 04-003-7133), with the size of $\sim$ 5 nm obtained using Scherer equation from peak at 43.7° (Fig. 4b inset).

Photovoltaic performance of QDSC with aerogels as electrolyte carrier

In order to fabricate the photocells, the BC, CNF, TOCNF and ChNF aerogel membranes were assembled together with the electrodes. Here, the membranes work as carrier of the electrolyte and to facilitate the ion-exchange. We evaluated the effect of the surface functional groups that were hypothesized to influence the performance of the photocells. All the aerogel membranes were freestanding and flexible and upon soaking them with the electrolyte, the respective system was easily sandwiched between the electrodes. Figure 5 shows the photocurrent–voltage (J–V) profiles of the cells under illumination corresponding to AM 1.5 G solar light, with an intensity of 1 full sun (100 mW cm^{-2}). The values of the traditional reference cell (with liquid

Fig. 4 **a** UV–Vis absorption spectra of CdS deposited on TiO$_2$ after several SILAR cycles; as indicated (0.1 M of Cd(NO$_3$)$_2$ and Na$_2$S, 60 s dipping time) and **b** XRD pattern of bare TiO$_2$ and CdS-sensitized TiO$_2$

Fig. 5 *J–V* curves of CdS-sensitized QDSCs with embedded biobased aerogels compared to the reference cell with liquid polysulfide electrolyte, under 1 Sun illumination

electrolyte) are reported for comparison (Fig. 5 and Table 2). It was observed that the cells including the aerogel membranes produced similar short-circuit current density (J_{sc}) and open circuit voltage (V_{oc}) despite of different surface functional groups. The performance of the membrane-embedded cells were also similar to that of reference cell without aerogels. The fill factor (FF) of the cells carrying the membranes was similar to each other, while slightly lower than that of membrane-free reference cell.

The recorded small fill factor suggested a charge transfer deficiency in the cell, identified in the EIS measurements to be caused by the poor charge transfer at the counter electrode/electrolyte interface; given the fact that the Pt catalyst is not an ideal catalyst for polysulfide electrolyte. In fact, the activity and conductivity of Pt-electrodes were known to be suppressed by adsorption of sulfur atoms (Yang et al. 2010; Soo Kang et al. 2015). It has been reported

that electrolyte reduction rate was higher on counter electrodes rather than Pt, such as metal sulfides (CuS, NiS) or carbon (graphene, carbon nanotubes), leading to a more rapid rate of hole recovery at counter electrode/electrolyte interface that accordingly improve J_{sc} and efficiency (Yang et al. 2010). In addition, the photocurrent was relatively low due to the recombination at the photoelectrode/electrolyte interface, attributed to the lack of blocking layer and slow hole-recovery rate of the electrolyte to the oxidized CdS-QDs (Lee and Chang 2008). Yang et al. reported that in a CdS-QD photoelectrode, addition of ZnS increased the efficiency almost double times, due to the elimination of charge recombination between the QDs and the electrolyte (Yang et al. 2010). The conversion power efficiency for the different aerogel-embedded QDSC showed values similar to that of the reference cell ($\sim$ 0.5%). Therefore, as the cells indicate similar performance, it means that the aerogels did not interfere with the cell operation nor with the charge transfer process in the electrolyte (further studied in "Interaction of polysulfide electrolyte with nanofibers" section). Considering the CdS-sensitized photoanode and Pt counter electrode, the obtained values for *CPE* and *FF* agree with the range reported in the literature (see Table 1) (Duan et al. 2014, 2015a). The photoanodes combined with different types of QDs (CdSe, CdSeTe, ZnS) and counter-electrodes other than Pt (carbon or metal sulfides) can lead to higher cell performance (Feng et al. 2016a, b; Jiang et al. 2016; Wei et al. 2016; Raphael et al. 2017); a subject that was not attempted here.

Electrochemical impedance spectroscopy (EIS) was performed in an equivalent circuit model including series resistance (R_s), an impedance at the electrolyte/electrode interface (R_{ct}) and the related

Table 2 Photovoltaic parameters of CdS-sensitized photocells with embedded biobased aerogel membranes as electrolyte retaining interface, compared to the traditional reference cell (with liquid polysulfide electrolyte), under 1 Sun illumination

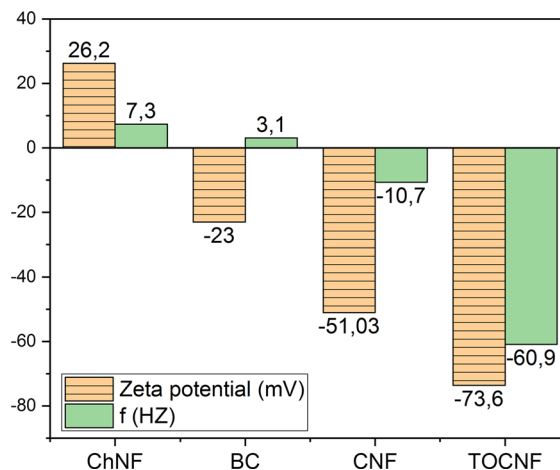| Electrolyte	J_{sc} (mA/cm^2)	V_{oc} (mV)	FF (%)	CPE (%)
Reference	4.8 ± 0.2	590 ± 2	20.3 ± 0.6	0.58 ± 0.01
BC	4.9 ± 0.2	583 ± 1	17.5 ± 1.2	0.50 ± 0.05
CNF	5.2 ± 0.5	558 ± 2	17.1 ± 0.2	0.52 ± 0.05
ChNF	5.0 ± 0.3	559 ± 8	16.4 ± 0.9	0.46 ± 0.01
TOCNF	5.1 ± 0.3	604 ± 4	17.1 ± 0.1	0.52 ± 0.03

capacitance C_{CPE}. The R_s described the Ohmic losses in the cells, typically from the resistances of the contacting layer and current collector contacts. R_s was very similar for all the cells (Table 3), which was expected since the conducting glass was the same for all the cells. Any difference in values were likely the result of the current collector contacts given that all preparations were made manually. R_{ct} defines the charge transfer resistance between the electrolyte and counter electrode, implying the reduction rate of polysulfide electrolyte on the Pt electrode. The higher values of R_{ct} indicates more internal voltage loss occurring at the counter electrode–electrolyte interface, leading to a lower FF and thus smaller values of conversion efficiency. As observed in Table 3, R_{ct} was quite similar in all the cells (105–145 Ω cm^2), yet much smaller than the values reported by Yang et al. (618 Ω cm^2) for similar polysulfide-Pt counter electrode system (Yang et al. 2010). Thus, it can be deduced that application of the bio-based membranes did not interfere with the charge transfer process.

Interaction of polysulfide electrolyte with nanofibers

QCM measurements were carried out in order to investigate the interactions between the electrolyte solution containing polysulfide ions and the functional groups present on the nanofiber surfaces. The frequency change (Δf) of the piezoelectric quartz crystals scales with the mass uptake (Encarna Ao et al. 2007). The dependence of frequency change upon injection and rinsing electrolyte over time is depicted in Fig. S4. The final frequency change of the modified QCM crystals with BC, CNF, TOCNF and ChNF after electrolyte rinsing was extracted from the formula in the supplementary information, and depicted in Fig. 6.

Table 3 Simulated values of resistance and capacitance from EIS measurements under 1 Sun illumination

Electrolyte	R_s (Ω)	R_{ct} (Ω cm^2)	C_{CPE} (μF cm^{-2})
Ref.	13	105	10.3
BC	12	138	25.8
CNF	11	112	35.9
ChNF	11	126	15.3
TOCNF	11	145	37.3

Fig. 6 Values of zeta-potential and the final frequency change after rinsing electrolyte from QCM crystals modified with BC, CNF, TOCNF, ChNF thin layers

It can be seen that the frequency change followed the trend of zeta potential, TOCNF > CNF > BC > ChNF. Much higher negative frequency change for the TOCNF film indicates a more extensive adsorption, given the more abundant carboxylate groups in this sample, which bind strongly with K$^+$ in the electrolyte. The higher negative surface charge of CNF compared to that of BC, mainly originated from the residual hemicelluloses in the former, which carry carboxyl groups on the surface that enhanced the adsorption of electrolyte cations. The amine groups on the surface of ChNF did not have affinity with the electrolyte cations nor polysulfide anions. The final dissipation value (Table S2) of TOCNF ($\sim$ 12) also imply that the films is a hydrated layer in its carboxylate from with potassium as counter ion, whereas low values for BC, CNF and ChNF (< 1) show that they were relatively unaffected.

It is known that the electrochemistry in polysulfide electrolytes is quite complex and the dissolution of sulfur in Na$_2$S leads to the formation of polysulfide (S_n^{2}) and supersulfide (S^{2-}) ions (Qian et al. 2013). In order to investigate whether the surface functional groups on the nanofibers influence the polysulfide redox reaction, electrochemical tests were carried out using cyclic voltammetry in a three-electrode cell system. Figure 7a shows CV of a bare GCE compared to TOCNF- and ChNF-coated GCE in stationary state (0 rpm). Two pairs of redox potentials were clearly observed in the voltammograms: a more positive peak
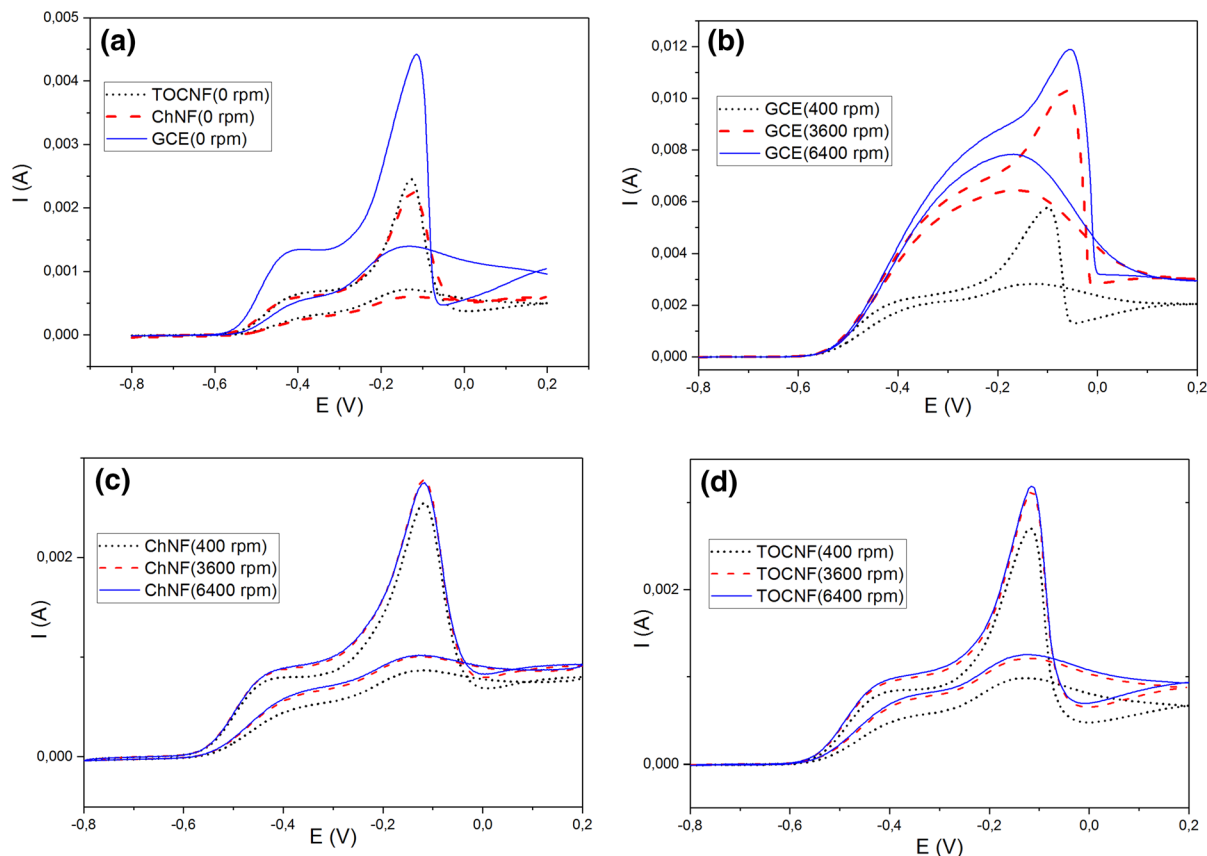
Fig. 7 CVs of bare GCE and coated GCE with TOCNF and ChNF in polysulfide electrolyte at **a** 0 rpm, **b** CVs of GCE in rotation state from 400 to 6400 rpm, **c** CVs of GCE coated with ChNF at different rotation rates and **d** CVs of GCE coated with TOCNF at different rotation rates

position corresponding the S/S^{2-} redox couple and a more negative one related to S^{2-}/S_n^{2-}. It is reported that S/S^{2-} redox reaction mainly occurs at the photoelectrode–electrolyte interface for the hole-re-covery, while S^{2-}/S_n^{2-} species are involved in electron exchange from the counter electrode (Yang et al. 2010). Evidently, the polysulfide reaction did not follow ideal Nernstian reaction, where the anodic and cathodic peak current, and positions are equal. It can be seen that the electrochemical behavior at the TOCNF- and ChNF-containing assembly were quite similar, despite their different surface functional groups. This suggests that the amine groups of ChNF and carboxylic groups of TOCNF did not interfere with the electrolyte redox reaction. However, in both cases, the redox peaks were smaller than those in bare GCE, which is explained by the fact that the redox couple have to permeate through the porous mem-branes. In rotating condition, the redox currents on

GCE increased significantly due to the elimination of mass-transfer diffusion (Vinodgopal et al. 2004). In accordance with the Levich equation, the limiting current increased proportionally with the rotation rates from 400 to 6400 rpm (Fig. 7b). However, there was no evidence of Levich behavior for both TOCNF- and ChNF-containing systems, and the obtained currents in rotating mode were close to those measured in the stationary system (Fig. 7c, d).

It can be inferred that a diffusion layer of the polysulfide ions formed inside the porous membranes and the redox couples may have been trapped so that the higher rotation rates could not overcome the mass-transfer resistance. Therefore, as illustrated in Fig. S5, the diffusion layer in the bare GCE is controlled by the rotation rate, whereas in the membrane-covered electrodes was not influenced by the rotation rates.

As observed in the voltammograms, the type of porous membranes and their different surface charges

did not influence the redox polysulfide reaction compared to the bare GCE. Considering the fact that the electrolyte in a solar cell is not flowing (in contrast to fuel cells), Fig. 7a resembles the electrolyte redox electrochemistry in the presence of biobased membranes in stationary form between electrodes. Besides, the redox peak positions did not change in the presence of biobased nanofibers, meaning that the redox reaction is occurring the similar way to the bare condition. This is in agreement with the data obtained in solar cell tests, where addition of different types of biobased membranes with different surface properties did not influence the cell performance. Therefore, considering the four types of biomaterials used in this work, BC could be more promising biobased aerogel due to its unique features (high purity, degree of polymerization and crystallinity) as well as economical benefits (Wu et al. 2016). Compared to CNF, TOCNF and ChNF that has to be obtained through procedures of top-down bleaching and fibrillation processing, BC can be obtained easily via microbial fermentation process even in industrial scale at a low cost.

Conclusions

Biobased aerogels were used as an environmentally friendly replacement for synthetic polymers as electrolyte carrier membranes in quantum dot-sensitized solar cell (QCSC). Bacterial cellulose (BC), cellulose nanofibers (CNF), chitin nanofibers (ChNF) and TEMPO-oxidized CNF (TOCNF) were selected due to different surface functional groups (hydroxyl, *N*-acetylglucosamine and carboxyl units) and their fibrilar structures that can form highly interconnected and robust network. It was observed that incorporation of biobased aerogels produced similar performance and the charge transfer resistance (R_{ct}) compared to the reference cell with liquid electrolyte, despite of different surface chemistry of the membranes. Interaction of biobased nanofibers with polysulfide electrolyte was investigated using quartz crystal microbalance (QCM), and showed no affinity to adsorb the polysulfide redox ions. Electrochemical measurements revealed that the respective functional groups did not influence the polysulfide redox reaction. Overall, there is indication that cellulose- and chitin-based materials, with their robust fibrilar

structure and high water-holding capability, are suitable renewable materials as polysulfide electrolyte membranes that can be promising alternatives to synthetic polymers, without interfering in the performance of the cell.

References

Chang JA, Rhee JH, Im SH et al (2010) High-performance nanostructured inorganic–organic heterojunction solar cells. Nano Lett 10:2609–2612. https://doi.org/10.1021/nl101322h

Chen HY, Lin L, Yu XY et al (2013) Dextran based highly conductive hydrogel polysulfide electrolyte for efficient quasi-solid-state quantum dot-sensitized solar cells. Electrochim Acta 92:117–123. https://doi.org/10.1016/j.electacta.2013.01.025

Du J, Meng X, Zhao K et al (2015) Performance enhancement of quantum dot sensitized solar cells by adding electrolyte additives. J Mater Chem A 3:17091–17097. https://doi.org/10.1039/C5TA04758G

Du C, Li H, Li B et al (2016) Characteristics and properties of cellulose nanofibers prepared by TEMPO oxidation of corn husk. BioResources 11:5276–5284. https://doi.org/10.15376/biores.11.2.5276-5284

Duan J, Tang Q, Sun Y et al (2014) Solid-state electrolytes from polysulfide integrated polyvinylpyrrolidone for quantum dot-sensitized solar cells. RSC Adv 4:60478–60483. https://doi.org/10.1039/C4RA10764K

Duan J, Tang Q, He B, Chen H (2015a) All-solid-state quantum dot-sensitized solar cell from plastic crystal electrolyte. RSC Adv 5:33463–33467. https://doi.org/10.1039/C5RA05275K

Duan J, Zhang H, Tang Q et al (2015b) Recent advances in critical materials for quantum dot-sensitized solar cells: a review. J Mater Chem A 3:17497–17510. https://doi.org/10.1039/C5TA03280F

Encarna Ao JM, Stallinga P, Ferreira GNM (2007) Influence of electrolytes in the QCM response: discrimination and quantification of the interference to correct microgravimetric data. Biosens Bioelectron 22:1351–1358. https://doi.org/10.1016/j.bios.2006.06.011

Feng W, Li Y, Du J et al (2016a) Highly efficient and stable quasi-solid-state quantum dot-sensitized solar cells

based on a superabsorbent polyelectrolyte. J Mater Chem A. https://doi.org/10.1039/C5TA08209A

Feng W, Zhao L, Du J et al (2016b) Quasi-solid-state quantum dot sensitized solar cells with power conversion efficiency over 9% and high stability. J Mater Chem A 4:14849–14856. https://doi.org/10.1039/C6TA05894A

Fujisawa S, Okita Y, Fukuzumi H et al (2011) Preparation and characterization of TEMPO-oxidized cellulose nanofibril films with free carboxyl groups. Carbohydr Polym 84:579–583. https://doi.org/10.1016/j.carbpol.2010.12.029

Hoeng F, Denneulin A, Bras J (2016) Use of nanocellulose in printed electronics: a review. Nanoscale 8:13131–13154. https://doi.org/10.1039/C6NR03054H

Huo Z, Tao L, Wang S et al (2015) A novel polysulfide hydrogel electrolyte based on low molecular mass organogelator for quasi-solid-state quantum dot-sensitized solar cells. J Power Sources 284:582–587. https://doi.org/10.1016/j.jpowsour.2015.03.049

Ifuku S, Nogi M, Abe K et al (2009) Preparation of chitin nanofibers with a uniform width as chitin from crab shells. Biomacromol 10:1584–1588. https://doi.org/10.1021/bm900163d

Jiang G, Pan Z, Ren Z et al (2016) Poly(vinyl pyrrolidone): a superior and general additive in polysulfide electrolytes for high efficiency quantum dot sensitized solar cells. J Mater Chem A 4:11416–11421. https://doi.org/10.1039/C6TA04027F

Kim H, Hwang I, Yong K (2014) Highly durable and efficient quantum dot-sensitized solar cells based on oligomer gel electrolytes. ACS Appl Mater Interfaces 6:11245–11253. https://doi.org/10.1021/am501407m

Kumar PN, Deepa M, Srivastava AK (2015) Ag plasmonic nanostructures and a novel gel electrolyte in a high efficiency TiO₂/CdS solar cell. Phys Chem Chem Phys 17:10040–10052. https://doi.org/10.1039/C4CP05820H

Larramona G, Choné C, Jacob A et al (2006) Nanostructured photovoltaic cell of the type titanium dioxide, cadmium sulfide thin coating, and copper thiocyanate showing high quantum efficiency. Chem Mater 18:1688–1696. https://doi.org/10.1021/cm052819n

Lee Y-L, Chang C-H (2008) Efficient polysulfide electrolyte for CdS quantum dot-sensitized solar cells. J Power Sources 185(1):584–588

Liang S, Zhang L, Xu J (2007) Morphology and permeability of cellulose/chitin blend membranes. J Membr Sci 287:19–28. https://doi.org/10.1016/j.memsci.2006.10.002

Miettunen K, Vapaavuori J, Tiihonen A et al (2014) Nanocellulose aerogel membranes for optimal electrolyte filling in dye solar cells. Nano Energy 8:95–102. https://doi.org/10.1016/j.nanoen.2014.05.013

Mingsukang M, Buraidah MH, Careem MA (2017) Development of gel polymer electrolytes for application in quantum dot-sensitized solar cells. Ionics (Kiel) 23:347–355. https://doi.org/10.1007/s11581-016-1895-7

Missoum K, Martoïa F, Belgacem MN, Bras J (2013) Effect of chemically modified nanofibrillated cellulose addition on the properties of fiber-based materials. Ind Crops Prod 48:98–105. https://doi.org/10.1016/j.indcrop.2013.04.013

Narayanan R, Deepa M, Srivastava AK (2013) Forster resonance energy transfer and carbon dots enhance light

harvesting in a solid-state quantum dot solar cell. J Mater Chem A 1:3907–3918. https://doi.org/10.1039/C3TA01601C

Orelma H, Vuoriluoto M, Johansson L-S et al (2016) Preparation of photoreactive nanocellulosic materials via benzophenone grafting. RSC Adv 6:85100–85106. https://doi.org/10.1039/C6RA15015B

Pathak P, Israel LH, Pereira EJM, Subramanian VR (2016) Effects of carbon allotrope interface on the photoactivity of rutile one-dimensional (1D) TiO₂ coated with anatase TiO₂ and sensitized with CdS nanocrystals. ACS Appl Mater Interfaces 8:13400–13409. https://doi.org/10.1021/acsami.6b01854

Qian L, Tian X, Yang L et al (2013) High specific capacitance of CuS nanotubes in redox active polysulfide electrolyte. RSC Adv 3:1703–1708. https://doi.org/10.1039/C2RA22257D

Raphael E, Jara DH, Schiavon MA (2017) Optimizing photovoltaic performance in CuInS₂ and CdS quantum dot-sensitized solar cells by using an agar-based gel polymer electrolyte. RSC Adv 7:6492–6500. https://doi.org/10.1039/C6RA27635K

Sehaqui H, Zhou Q, Berglund LA (2011) High-porosity aerogels of high specific surface area prepared from nanofibrillated cellulose (NFC). Compos Sci Technol 71:1593–1599. https://doi.org/10.1016/j.compscitech.2011.07.003

Sharma HSS, Carmichael E, Muhamad M et al (2012) Biorefining of perennial ryegrass for the production of nanofibrillated cellulose. RSC Adv 2:6424. https://doi.org/10.1039/c2ra20716h

Sharma D, Jha R, Kumar S (2016) Quantum dot sensitized solar cell: recent advances and future perspectives in photoanode. Sol Energy Mater Sol Cells 155:294–322. https://doi.org/10.1016/j.solmat.2016.05.062

Shen C, Fichou D, Wang Q (2016) Interfacial engineering for quantum-dot-sensitized solar cells. Chem Asian J 11:1183–1193. https://doi.org/10.1002/asia.201600034

Soo Kang J, Park M-A, Kim J-Y et al (2015) Reactively sputtered nickel nitride as electrocatalytic counter electrode for dye- and quantum dot-sensitized solar cells. Sci Rep 5:10450. https://doi.org/10.1038/srep10450

Toivonen MS, Kaskela A, Rojas OJ et al (2015) Ambient-dried cellulose nanofibril aerogel membranes with high tensile strength and their use for aerosol collection and templates for transparent, flexible devices. Adv Funct Mater 25:6618–6626. https://doi.org/10.1002/adfm.201502566

Vinodgopal K, Subramanian V, Kamat PV (2004) Selective electrochemical detection of ionic and neutral species using films of Suwannee river humic acid. Environ Sci Technol 38:2161–2166. https://doi.org/10.1021/es034988j

Wang S, Zhang QX, Xu YZ et al (2013) Single-step in situ preparation of thin film electrolyte for quasi-solid state quantum dot-sensitized solar cells. J Power Sources 224:152–157. https://doi.org/10.1016/j.jpowsour.2012.09.044

Wei H, Wang G, Shi J et al (2016) Fumed SiO₂ modified electrolytes for quantum dot sensitized solar cells with efficiency exceeding 11% and better stability. J Mater Chem A 14:115. https://doi.org/10.1039/C6TA04570G

Wu Z-Y, Liang H-W, Chen L-F et al (2016) Bacterial cellulose: a robust platform for design of three dimensional carbon-based functional nanomaterials. Acc Chem Res 49:96–105

Xia J, Masaki N, Lira-Cantu M et al (2008) Influence of doped anions on poly(3,4-ethylenedioxythiophene) as hole conductors for iodine-free solid-state dye-sensitized solar cells. J Am Chem Soc 130:1258–1263. https://doi.org/10.1021/ja075704o

Yang Y, Wang W (2015) A new polymer electrolyte for solid-state quantum dot sensitized solar cells. J Power Sources 285:70–75. https://doi.org/10.1016/j.jpowsour.2015.03.061

Yang Z, Chen C-Y, Liu C-W, Chang H-T (2010) Electrocatalytic sulfur electrodes for CdS/CdSe quantum dot-sensitized solar cells. Chem Commun 46:5485. https://doi.org/10.1039/c0cc00642d

Yu Z, Zhang Q, Qin D et al (2010) Highly efficient quasi-solid-state quantum-dot-sensitized solar cell based on hydrogel electrolytes. Electrochem Commun 12:1776–1779. https://doi.org/10.1016/j.elecom.2010.10.022

Zhou Y, Fuentes-Hernandez C, Khan TM et al (2013) Recyclable organic solar cells on cellulose nanocrystal substrates. Sci Rep 3:1536. https://doi.org/10.1038/srep01536

Zhu H, Fang Z, Preston C et al (2014) Transparent paper: fabrications, properties, and device applications. Energy Environ Sci 7:269–287. https://doi.org/10.1039/C3EE43024C

Zhu M, Li T, Davis CS et al (2016) Transparent and haze wood composites for highly efficient broadband light management in solar cells. Nano Energy 26:332–339